Rock Mech Rock Eng (2017) 50:665–674
DOI 10.1007/s00603-016-1165-z

ISRM SUGGESTED METHOD

ISRM Suggested Method for Laboratory Acoustic Emission Monitoring

Tsuyoshi Ishida[1] · Joseph F. Labuz[2] · Gerd Manthei[3] · Philip G. Meredith[4] · M. H. B. Nasseri[5] · Koichi Shin[6] · Tatsuya Yokoyama[7] · Arno Zang[8]

1 Introduction

Acoustic emission (AE) is defined as high-frequency elastic waves emitted from defects such as small cracks (microcracks) within a material when stressed, typically in the laboratory. AE is a similar phenomenon to microseismicity (MS), as MS is induced by fracture of rock at an engineering scale (e.g., rockbursts in mines), that is, in the field. Thus, seismic monitoring can be applied to a wide variety of rock engineering problems, and AE is a powerful method to investigate processes of rock fracture by detecting microcracks prior to macroscopic failure and by tracking crack propagation.

A basic approach involves using a single channel of data acquisition, such as with a digital oscilloscope, and analyzing the number and rate of AE events. Perhaps the most valuable information from AE is the source location, which requires recording the waveform at several sensors and determining arrival times at each. Thus, investing in a multichannel data acquisition system provides the means to monitor dynamics of the fracturing process.

The purpose of this suggested method is to describe the experimental setup and devices used to monitor AE in laboratory testing of rock. The instrumentation includes the AE sensor, preamplifier, frequency (noise) filter, main amplifier, AE rate counter, and A/D (analog-to-digital) recorder, to provide fundamental knowledge on material and specimen behavior in laboratory experiments. When considering in situ seismic monitoring, the reader is referred to the relevant ISRM suggested method specifically addressing that topic (Xiao et al. 2016).

2 Brief Historical Review

2.1 Early Studies of AE Monitoring for Laboratory Testing

AE/MS monitoring of rock is generally credited to Obert and Duval (1945) in their seminal work related to predicting rock failure in underground mines. Laboratory testing was later used to understand better the failure process of rock (Mogi 1962a). For example, the nature of crustal-scale earthquakes from observations of microscale

Please send any written comments on this Suggested method to Prof. Resat Ulusay, President of the ISRM Commission on Testing Methods, Hacettepe University, Department of Geological Engineering, 06800 Beytepe, Ankara, Turkey. E-mail: resat@hacettepe.edu.tr

✉ Tsuyoshi Ishida
ishida.tsuyoshi.2a@kyoto-u.ac.jp

[1] Department of Civil and Earth Resources Engineering, Kyoto University, C-Cluster, Katsura Campus of Kyoto University, Nishikyo-ku, Kyoto 615-8540, Japan

[2] Department of Civil, Environmental and Geo-Engineering, University of Minnesota, Minneapolis, MN 55455, USA

[3] THM University of Applied Sciences, Wiesenstraße 14, 35390 Giessen, Germany

[4] Department of Earth Sciences, University College London, Gower Street, London WC1E 6BT, UK

[5] Department of Civil Engineering, University of Toronto, 35 St. George Street, Toronto, ON M5S 1A4, Canada

[6] Central Research Institute of Electric Power Industry, 1646 Abiko, Abiko-city, Chiba-prefecture 270-1194, Japan

[7] Engineering Headquarters, OYO Corporation, 2-2-19 Daitakubo, Minami-ku, Saitama 336-0015, Japan

[8] Section 2.6, Seismic Hazard and Stress Field, Helmholtz-Zentrum Potsdam, German Research Center for Geosciences-GFZ, Telegrafenberg, 14473 Potsdam, Germany

fracture phenomena was a popular topic. Mogi (1968) discussed the process of foreshocks, main shocks, and aftershocks from AE activity monitored through failure of rock specimens. Scholz (1968b, c) studied the fracturing process of rock and discussed the relation between microcracking and inelastic deformation. Nishizawa et al. (1984) examined focal mechanisms of microseismicity, and Kusunose and Nishizawa (1986) discussed the concept of the seismic gap from AE data obtained in their laboratory experiments. Spetzler et al. (1991) discussed stick-slip events in pre-fractured rock with various surface roughness by combining acoustic emission with holographic interferometry measurements. Compiling years of study, Scholz (2002) and Mogi (2006) published books on rock failure processes from a geophysics perspective. Hardy (1994, 2003) focused on geoengineering applications of AE, while Grosse and Ohtsu (2008) edited topics on the use of AE as a health monitoring method for civil engineering structures.

2.2 AE Monitoring in Novel Applications

Many researchers have used AE in novel ways. Yanagidani et al. (1985) performed creep experiments under constant uniaxial stress and used AE location data to elucidate a cluster of microcracks prior to macroscale faulting. His research group also developed the concept of using AE rate to control compression experiments (Terada et al. 1984). Using this method, Lockner et al. (1991) conducted laboratory experiments under controlled loading by keeping the AE rate constant and discussed the relation between fault growth and shear fracture by imaging AE nucleation and propagation.

Besides the research on rock fracturing, AE monitoring has been applied to stress measurement using the Kaiser effect (1953), that is, the stress memory effect with respect to AE occurrence in rock. This application was started by Kanagawa et al. (1976) and patented by Kanagawa and Nakasa (1978). Lavrov (2003) presented a historical review of the approach.

2.3 AE Monitoring with Development of Digital Technology

With development of digital technology, AE instrumentation advanced through the use of high-speed and large-capacity data acquisition systems. For example, using non-standard asymmetric compression specimens, Zang et al. (1998, 2000) located AE sources, analyzed the fracturing mechanism, and compared the results with images of X-ray CT scans. Studies of the fracture process zone include Zietlow and Labuz (1998), Zang et al. (2000), and Nasseri et al. (2006), among others. Benson et al. (2008) conducted a laboratory experiment to simulate volcano seismicity and observed low-frequency AE events exhibiting a weak component of shear (double couple) slip, consistent with fluid-driven events occurring beneath active volcanoes. Heap et al. (2009) conducted stress-stepping creep tests under pore fluid pressure and discussed effects of stress corrosion using located AE data. Chen and Labuz (2006) performed indentation tests of rock using wedge-shaped tools and compared the damage zone shown with located AE sources to theoretical predictions.

Ishida et al. (2004, 2012) conducted hydraulic fracturing laboratory experiments using various fluids, including supercritical carbon dioxide, and discussed differences in induced cracks due to fluid viscosity using distributions of AE sources and fault plane solutions. Using AE data from triaxial experiments, Goebel et al. (2012) studied stick-slip sequences to gain insight into fault processes, and Yoshimitsu et al. (2014) suggested that both millimeter scale fractures and natural earthquakes of kilometer scale are highly similar as physical processes. The similarity is also supported by Kwiatek et al. (2011) and Goodfellow and Young (2014).

Moment tensor analysis of AE events has been applied to laboratory experiments. Shah and Labuz (1995) and Sellers et al. (2003) analyzed source mechanisms of AE events under uniaxial loading, while Graham et al. (2010) and Manthei (2005) analyzed them under triaxial loading. Kao et al. (2011) explained the predominance of shear microcracking in mode I fracture tests through a moment tensor representation of AE as displacement discontinuities.

3 Devices for AE Monitoring

One of the simplest loading arrangements for AE monitoring in the laboratory is that for uniaxial compression of a rock specimen; Fig. 1 shows a typical arrangement. Since an AE signal detected at a sensor is of very low amplitude, the signal is amplified through a preamplifier and possibly a main amplifier. Typically the signal travels through a

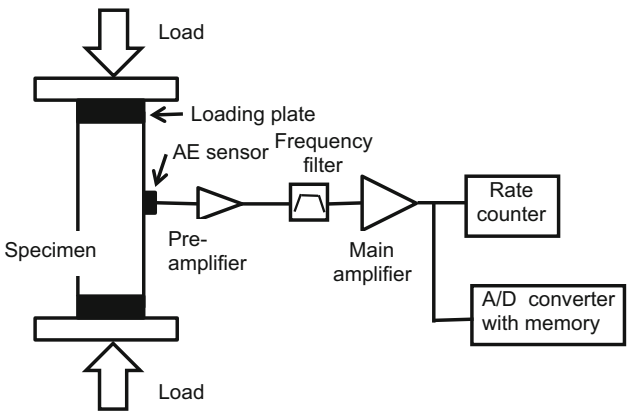

Fig. 1 Typical AE monitoring system for a laboratory uniaxial compression test

coaxial cable (a conductor with a wire mesh to shield the signal from electromagnetically induced noise) with a Bayonet Neill Concelman (BNC) connector. It is usually necessary to further eliminate noise, so a band-pass filter, a device that passes frequencies within a certain range, is used. In the most basic setup using one sensor only, the rate of AE events is counted by processing the detected signals. In more advanced monitoring, for example, for source location of AE events, more sensors are used and AE waveforms detected at the respective sensors are recorded through an A/D converter. Figure 2a shows a twelve-sensor array for a core 50 mm in diameter and 100 mm in length (Zang et al. 2000); an AE rate-controlled experiment was performed to map a fracture tip by AE locations, as shown in Fig. 2b. To locate AE, it is advantageous for the sensors to be mounted so as to surround the source, as shown in Fig. 2. The three lines indicate paths to monitor P waves transmitted from sensor No. 12 by using it as an emitter.

3.1 AE Sensor

AE sensors are typically ceramic piezoelectric elements. The absolute sensitivity is defined as the ratio of an output electric voltage to velocity or pressure applied to a sensitive surface of a sensor in units, V/(m/s) or V/kPa, and its order is 0.1 mV/kPa. However, the absolute sensitivity often depends on the calibration method (McLaskey and Glaser 2012). For this reason, a sensitivity of an AE sensor is usually stated as relative sensitivity in units of dB.

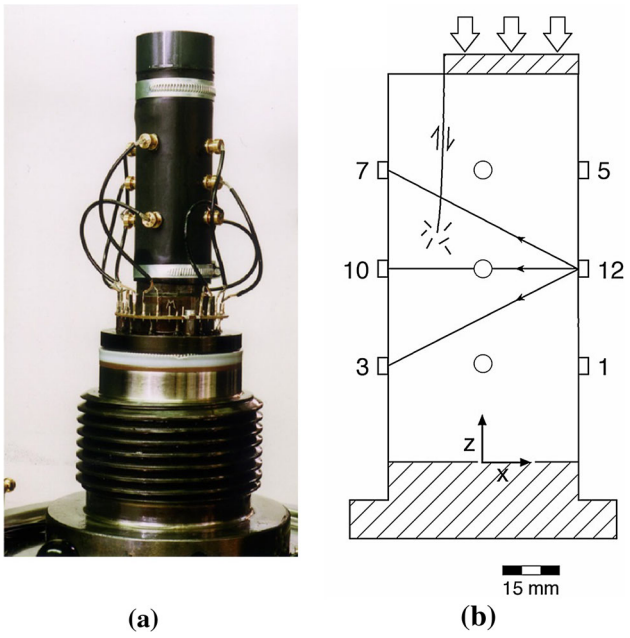

Fig. 2 Example of the twelve-sensor array for a core measuring 5 cm in diameter and 10 cm in length after Zang et al. (2000). **a** Photograph, **b** illustration

Figure 3 shows a typical sensor with a preamplifier. AE sensors can be classified into two types, depending on frequency characteristics: resonance and broadband. Figure 4a illustrates the frequency response of a resonance-type sensor, while Fig. 4b shows the characteristics of a broadband-type sensor. Both sensors have a cylindrical shape with the same size of 18 mm in diameter and 17 mm in height. However, it can be seen that the resonance-type sensor (Fig. 4a) has a clear peak around 150 kHz while the broadband type (Fig. 4b) has a response without any clear peak from 200 to 800 kHz. Since the resonance type detects an AE event at the most sensitive frequency, it tends to produce a signal having large amplitude in a frequency band close to its resonance frequency, independent of a dominant frequency of the actual AE waveform. As a result, the resonance-type sensor conceals the characteristic frequency of the "actual" AE signal, and it may lose important information about the source.

On the other hand, it is often claimed that the broadband type records a signal corresponding to the original waveform. However, comparing Fig. 4a and b illustrates that the sensitivity of the broadband type is on average 10 dB less than that of the resonance type. For this reason, the resonance-type sensor is often employed for AE monitoring. In an early study on rock fracturing (Zang et al. 1996), both sensor types, resonance and broadband, were used to investigate fracture mechanisms in dry and wet sandstone. Further, broadband sensors have been developed to provide high fidelity signals for source characterization (Proctor 1982; Boler et al. 1984; Glaser et al. 1998; McLaskey and Glaser 2012; McLaskey et al. 2014). One additional item that should be noted is that sensor selection should be dependent on rock type. For weak rock like mudstone having low stiffness and high attenuation, an AE sensor having a lower resonance frequency is recommended because it is difficult to monitor high-frequency signals in a weak rock.

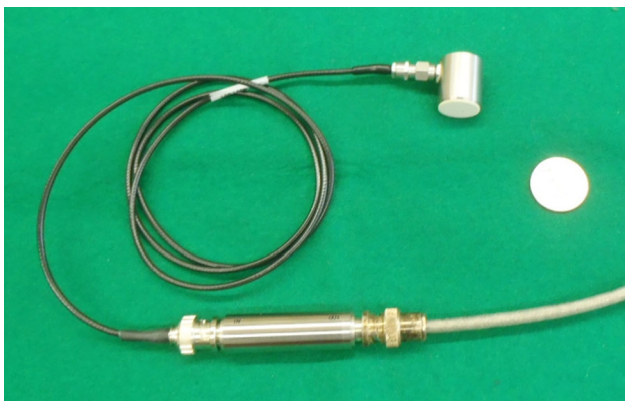

Fig. 3 Typical AE sensor and preamplifier for a laboratory experiment. Coin is 24.26 mm in diameter (a quarter of US dollar) for scale

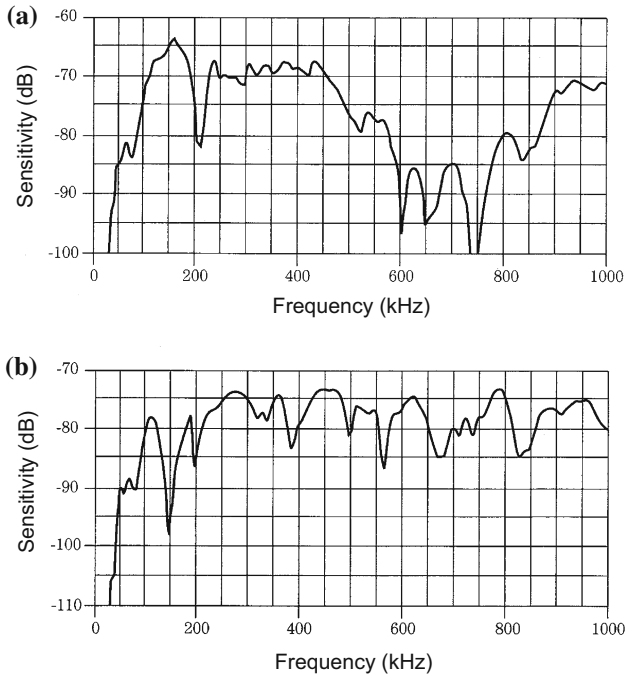

Fig. 4 Examples of frequency response characteristics of AE sensors. **a** Resonance-type sensor, PAC Type R15 with a resonance frequency 150 kHz. **b** Broadband-type sensor, PAC Type UT1000. Both sensor models from Physical Acoustics Corporation, Princeton, NJ, USA

For counting AE events, two or more sensors should be used to check the effect of sensor position and distinguish AE signals from noise. For 3D source locations of AE events, at least five sensors (or four sensors and one other piece of information) are necessary, because of the four unknowns (source coordinates x, y, z, and an occurrence time t) and the quadratic nature of the distance equation. More than eight sensors are usually used to improve the locations of the AE events through an optimization scheme (Salamon and Wiebols 1974).

For setting an AE sensor on a cylindrical specimen, it is recommended to machine a small area of the curved surface to match the planar end of the sensor. To adhere the sensor on the specimen, various kinds of adhesives can be used, such as a cyanoacrylate-based glue or even wax, which allows easy removal. It is recommended to use a consistent but small amount of adhesive so as to reduce the coupling effect (Shah and Labuz 1995). Many AE sensors are designed to operate within a pressure vessel, so from the perspective of the AE technique, the issues are the same for uniaxial and triaxial testing.

3.2 Amplifiers and Filters

When AE events generated in a specimen are detected by an AE sensor, the motion induces an electric charge on the piezoelectric element. A preamplifier connected to the AE sensor transfers the accumulated electric charge as a voltage signal with a gain setting from 10 to 1000 times. Thus, a preamplifier should be located within close proximity (<1 m) from an AE sensor, and some commercial AE sensors are equipped with integrated preamplifiers. Since a preamplifier needs a power supply to amplify a signal, it is should be connected to a "clean" power unit so that the signal is not buried in noise.

A signal amplified by a preamplifier is often connected to another amplifier, and a frequency filter is inserted to reduce noise. A high-pass filter passes only a signal having frequencies higher than a set frequency to eliminate the lower-frequency noises; a low-pass filter eliminates the higher-frequency noise. A filter that combines the two is called a band-pass filter and is often used as well. When the AE sensor shown in Fig. 3 having a resonance frequency of 150 kHz is employed, a band-pass filter from 20 to 2000 kHz is common. A band frequency of the filter should be selected depending on the frequency of the anticipated waves and on the frequency of the noise.

3.3 AE Count and Rate

The AE count is associated with the number of AE, whereas the AE count rate is based on the AE count per unit time. Figure 5 shows a typical example of AE count rates monitored in a uniaxial compression test on a rock core. It is possible to show a relation between impending failure and AE occurrence, when AE count rates are shown with a load–displacement curve. Noting that the AE count rate on the y-axis is plotted on a logarithmic scale, a burst of AE is observed just before failure (peak axial stress) of the specimen. This suggests that AE count rate is a sensitive parameter for observing failure.

Methods to determine AE counts are classified into ring-down count and event count. In both cases, a certain voltage level called the threshold or discriminate level is set for AE recording (Fig. 6). The level is set slightly higher than the background noise level regardless of rock properties and test conditions, and consequently the AE count and rate depend on the threshold level. In a ring-down counting method, a transistor–transistor logic (TTL) signal is produced every time a signal exceeds a threshold level. In the case shown in Fig. 6b, five TTL signals are produced for one AE event, and they are sent to a counter as five counts. On the other hand, an event count records one count for each AE event; a typical method generates a low-frequency signal that envelopes the original signal (Fig. 6c). After that, when the low-frequency signal exceeds a threshold level, one TTL signal is produced and sent to a counter. The function to generate the TTL signals should be mounted in a main amplifier or a rate counter as shown in Fig. 1.

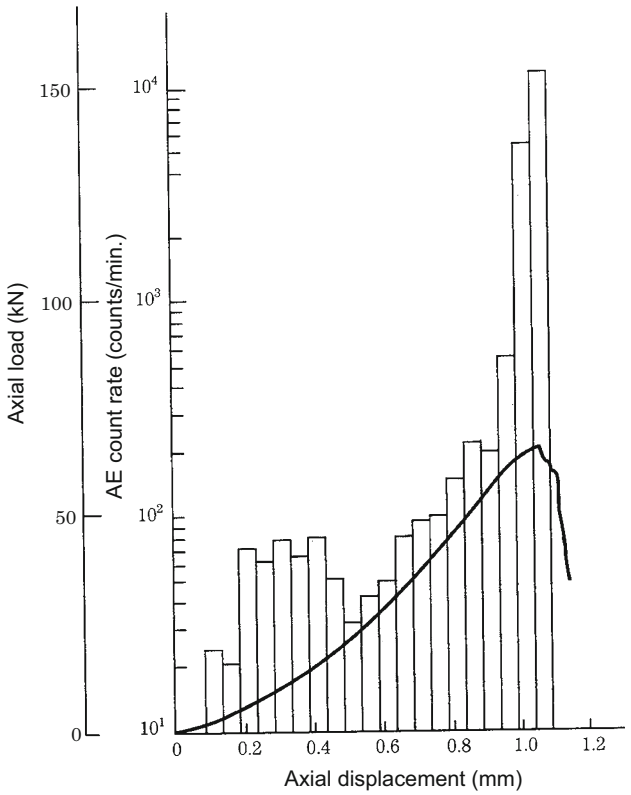

Fig. 5 Typical AE count rate monitored in a uniaxial compression test under a constant axial displacement rate. The *bar graph* and the *bold line* indicate AE count rates and the load–displacement curve, respectively

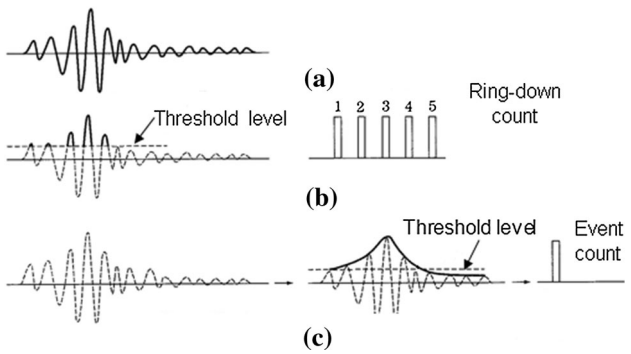

Fig. 6 Two methods to count AE events. **a** Original AE waveform. **b** Ring-down count. **c** Event count

Whichever method is selected, AE counts and rates depend on the gain of the amplifiers and the threshold level. Thus, the threshold level should be reported together with the respective gains of the preamplifier and amplifier, along with the method selected for counting. Nonetheless, comparison of AE counts and rates between two experiments should be done cautiously, as the failure mechanism, or more importantly, coupling may differ. Sensitivity of an AE sensor is strongly affected by the coupling condition between the sensor and specimen. For example, the area and shape of the couplant (adhesive) can be different, even if the couplant is applied in the same manner (Shah and Labuz 1995). For these reasons, comparison of exact numbers of AE counts and rates between two experiments is not recommended, although their changes within an experiment become very good indices for identifying the accumulation of damage and extension of fracture.

3.4 Recording AE Waveforms

AE waveforms contain valuable information on the fracture process, including location of the AE source. AE waveforms can be recorded by an A/D converter and stored in memory.

1. Principle of A/D conversion

To record an AE waveform, as shown in Fig. 7, an electric signal from an AE sensor flows through an A/D converter. When the amplitude of the signal exceeds a threshold level, which is set in advance, a certain "length" of the signal before and after the threshold is stored in memory. While the voltage level set in advance is called the threshold level or discriminate level, the time when a signal voltage exceeds the level is called the trigger time or trigger point. Note that "trigger" can mean either to start a circuit or to change the state of a circuit by a pulse, while, in some cases, "trigger" means the pulse itself. In actual monitoring, the TTL signal for the AE rate counter is usually branched and connected into an A/D converter as the trigger signal. Sometimes, to avoid recording waveforms that cannot provide sufficient information to determine a source location, a logic of AND/OR for triggering is used;

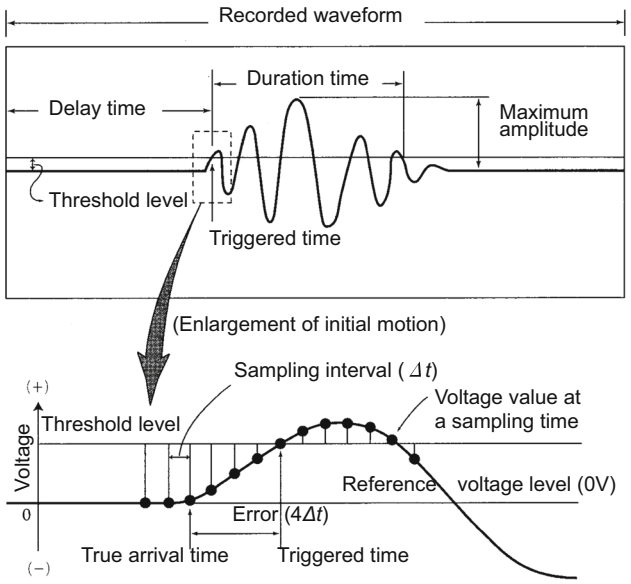

Fig. 7 Example of recorded AE waveform and illustration of its analog/digital conversion

for example, triggering occurs only when signals of two sensors set in the opposite position on the specimen exceed a threshold level at the same time. Indeed, it is possible to use much more complex logic. Using an arrival time picking algorithm, automatic source location of AE events can be realized.

When recording an AE waveform, a time period before the trigger time needs to be specified and this time period is called the pre-trigger or delay time. In A/D conversion, voltages of an analog signal are read with a certain time interval and the voltages are stored in memory as digital numbers. The principle is illustrated in an enlarged view of an initial motion of the waveform in the lower part of Fig. 7. The time interval, Δt, is called the sampling time. On the other hand, the recording time of a waveform is sometimes designated as a memory length of an A/D converter.

For example, in an hydraulic fracturing experiment on a 190-mm cubic granite specimen (Ishida et al. 2004) and a uniaxial loading experiment on a 300 × 200 × 60 mm rectangular tuff specimen (Nakayama et al. 1993), the researchers used a sensor having a resonance frequency of 150 kHz, which is shown in Fig. 3, and monitored AE signals by using a sampling time of 0.2 μs and a memory length of 2 k (2048 words). In this case, the recording time period was around 0.4 ms (0.2 μs × 2048). The pre-trigger was set at 1 k, one-half of the recording time; the pre-trigger is often reported as memory length rather than in real time.

2. Sampling time

To explain selection of a proper sampling time, consider the case where a sine curve is converted at only four points from analog data to digital. If the sampling points meet the maximum and the minimum points of the curve, as shown in Fig. 8a, a signal reproduced by linear interpolation from the converted digital data is similar to the original signal.

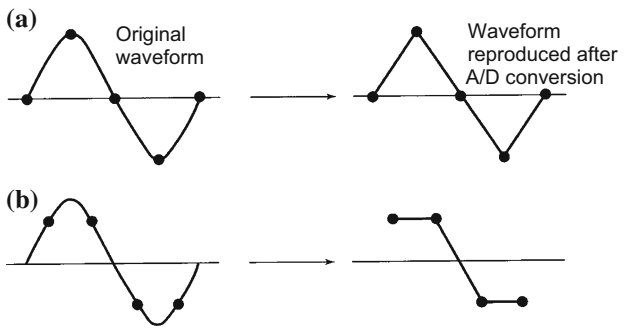

Fig. 8 Relationship between an original waveform and a waveform reproduced after A/D conversion. **a** Sampling points meet the maximum and the minimum points of the original waveform. **b** Sampling points are displaced 1/8 cycle along the time axis

However, if the sampling points are moved 1/8 cycle along the time axis, as shown in Fig. 8b, the reproduced signal is much distorted from the original one. These two examples suggest that four sampling points for a cycle are not sufficient and at least ten points for a cycle are needed to reproduce the waveform correctly from the converted digital data.

A specification of an A/D converter usually shows a reciprocal number of the minimum sampling time. For example, if the minimum sampling time is 1 μs, the specification shows the reciprocal number, 1 MHz, as the maximum monitoring frequency. However, this does not mean the frequency of a waveform that can be correctly reproduced. In this case, around one-tenth of the frequency, or 100 kHz, can be recorded.

3. Resolution of amplitude

Whereas the sampling time corresponds to the resolution along the x-axis of an A/D converter, the resolution capability along the y-axis (amplitude), usually called dynamic range, is the range from the discriminable or the resolvable minimum voltage difference to the recordable maximum voltage, and it depends on the bit length. When the length is 8 bits, its full scale, for example, from −1 to +1 V, is divided into $2^8 = 256$. Thus, in this case, any differences smaller than 2/256 volts in the amplitude are automatically ignored. If the bit length is 16 bits, the full scale from −1 to +1 V is divided into $2^{16} = 65{,}536$ and much smaller differences can be discriminated. The dynamic range is from 7.8×10^{-3}(=2/256) to 2 V for 8 bits, whereas it is from 3.1×10^{-5}(=2/65,536) to 2 V for 16 bits.

When using amplitude data of the waveform in analysis, for example, to calculate the b value using the Gutenberg–Richter relation (Gutenberg and Richter 1942), a large dynamic range is essential. The unit "word" of a recording length is sometimes used, noting that one word corresponds to 8 bits (1 byte) where the bit length is 8 bits, whereas it corresponds to 16 bits (2 bytes) for a case of 16 bits.

4. Continuous AE acquisition

A conventional transient recording system has a certain dead time for transferring data, where AE are not recorded during this interval; this could result in loss of valuable information, especially in the case of a high level of AE activity. Continuous AE acquisition systems record without data loss, but the disadvantage of such systems is the huge dataset, requiring additional software for processing. With the increase in installed memory, systems that can record all AE events continuously through an experiment have become commercially available. Since some researchers have already started to use this type of system, continuous monitoring (without trigger) may become increasingly popular in the near future.

The following examples show the capability of continuous AE acquisition. A continuous recorder was used to record 0.8 s at 10 MHz and 16 bits (Lei et al. 2003). A continuous AE recorder was used to store 268 s of continuous AE data on 16 channels at a sampling rate of 5 MHz and at 14-bit resolution (Thompson et al. 2005, 2006; Nasseri et al. 2006). A more advanced continuous AE acquisition system, which can record continuously for hours at 10 MHz and 12 or 16 bits, was used within conventional triaxial and true-triaxial geophysical imaging cells (Benson et al. 2008; Nasseri et al. 2014). In addition, there exists a combined system with the capability for conventional transient recording when there is a low AE activity and for recording AE continuously in the case of a high level of AE activity; this provides zero dead time and avoids the loss of AE signals (Stanchits et al. 2011). A disadvantage of such a system is that it costs more than a conventional transient or a continuously recording system.

4 Analysis

AE data analysis can be classified into the four categories: (1) event count and rate, (2) source location, (3) energy release and the Gutenberg–Richter relation, and (4) source mechanism. In this section, AE data analysis is explained in this order.

4.1 Event Counting

The most basic type of AE data analysis involves counting events as a function of time. As shown in Fig. 5, by comparing AE rates with change of stress, strain, or other measured quantity characterizing the response, valuable insight on the accumulation of damage and extension of fracture can be obtained. Various statistical modeling methods can be used to extract additional information, including the Kaiser effect (Lockner 1993; Lavrov 2003).

4.2 Source Location

If waveforms of an AE event are recorded at a number of sensors, the source can be located, providing perhaps the most valuable information from AE. Different approaches can be taken to determine source locations of AE events, but a common approach is to use a nonlinear least squares method to seek four unknowns, the source coordinates x, y, z, and an occurrence time t, knowing the P wave arrival time at each sensor and the P wave velocity measured before the experiment under the assumption that it does not change through the experiment. A seminal contribution to the source location problem is the paper by Salamon and Wiebols (1974). Other valuable references include Section 7.2 of Stein and Wysession (2003) and Section 5.7 of Shearer (2009). Source locations of AE events in laboratory experiments are reported in many papers (Lei et al. 1992; Zang et al. 1998, 2000; Fakhimi et al. 2002; Benson et al. 2008; Graham et al. 2010; Stanchits et al. 2011, 2014; Ishida et al. 2004, 2012; Yoshimitsu et al. 2014). In addition, the calculation of fractal dimension using spatial distributions of AE sources can be quite valuable in identifying localization (Lockner et al. 1991; Lei et al. 1992; Shah and Labuz 1995; Zang et al. 1998; Lei et al. 2003; Stanchits et al. 2011).

4.3 Energy Release and the Gutenberg–Richter Relation

A signal recorded at only one sensor should not be used to estimate energy released due to geometric attenuation of the signal. However, for a large number of sensors with sufficient coverage, an average root-mean-square (RMS) value from all the sensors will be representative of the AE energy. The RMS value is obtained by taking the actual voltage $g(t)$ at each point along the AE waveform and averaging the square of $g(t)$ over the time period T; the square root of the average value gives the RMS value.

The Gutenberg–Richter relationship, originally proposed as a relation between magnitudes of earthquakes and their numbers, can also be applied to AE data. Mogi (1962a, b) indicated through his laboratory experiments that the relation depends on the degree of heterogeneity of the material. Scholz (1968a) found in uniaxial and triaxial compression tests that the state of stress, rather than the heterogeneity of the material, plays the most important role in determining the relation. These findings have been applied to understand the phenomena of earthquakes, and the Gutenberg–Richter relationship is often used as an index value for fracturing in rock specimens (Lei et al. 1992, 2003; Lockner 1993; Zang et al. 1998; Stanchits et al. 2011).

4.4 Source Mechanism

If the polarity of the initial P wave motion at several sensors is identified, the source mechanism can be analyzed using a fault plane solution. The polarity of a waveform is defined as positive if the first motion is compressive or outward and negative if it is tensile or inward. Microcrack opening and volumetric expansion mechanisms cause positive first motions in all the directions around the source, whereas microcrack closing and pore collapse mechanisms cause all negative first motions. A pure sliding mechanism causes equal distributions of positive and negative polarities. The distribution of polarities for a

mixed-mode mechanism (e.g., sliding with dilation) is more complex. Since the theory applied to seismology can be directly applied to AE owing to the same physical mechanism of fracturing, the approach is described in several seismology texts, including Chapter 3 of Kasahara (1981), Section 4.2 of Stein and Wysession (2003), and Chapter 9 of Shearer (2009). The fault plane solutions of AE events in laboratory experiments are reported in Lei et al. (1992), Zang et al. (1998), and Benson et al. (2008).

With proper sensor calibration and simplifying assumptions (Davi et al. 2013; Kwiatek et al. 2014; Stierle et al. 2016), a detailed analysis of the source mechanism using the concept of the moment tensor can be performed. The AE source is characterized as a discontinuity in displacement, a microcrack, and represented by force dipoles that form the moment tensor. An inverse problem is solved for the six components of the moment tensor, which are then related to the physical quantities of microcrack displacement and orientation. In general, the directions of the displacement vector and the normal vector of the microcrack can be interchanged, but an angle 2α between the two vectors indicates opening when $\alpha = 0°$, sliding when $\alpha = 45°$, and anything in between is mixed mode. The theory is reviewed in seismology texts, e.g., Section 4.4 of Stein and Wysession (2003) and Chapter 9 of Shearer (2009), as well as in papers by Ohtsu and Ono (1986), Shah and Labuz (1995), and Manthei (2005). Applications of the moment tensor analysis to model AE events as microcracks are found in Kao et al. (2011), Davi et al. (2013), Kwiatek et al. (2014), and Stierle et al. (2016).

4.5 Reporting of Results

A report on AE laboratory monitoring should include the following:

1. Size, shape, and rock type of the specimen.
2. Size and frequency of the sensor and type (resonance or broadband).
3. Number of AE sensors used and sensor arrangement.
4. Block diagram of AE monitoring system or explanation of its outline.
5. Gain of pre- and main- amplifier of each channel.
6. Setting frequencies of high-pass and low-pass filter of each channel.
7. Threshold level of each channel for count rate and/or trigger for waveform recording.
8. If a triggering system is used, how to select AE sensors and how to use logical AND/OR for triggering. Dead time or continuous AE acquisition should be stated as well.
9. Sampling time, memory length (recording time period of each waveform), pre-trigger time and resolution of amplitude, if waveform is recorded.
10. Analysis of results, for example, AE count rate as a function of time, location of AE events, mechanisms of AE events including fault plane, moment tensor, or other solutions.
11. Other measured quantities related to the purpose of the experiment, for example, stress, strain, pressure, and temperature, should be reported in comparison with the AE data.

References

Benson PM, Vinciguerra S, Meredith PG, Young RP (2008) Laboratory simulation of volcano seismicity. Science 332(10):249–252

Boler FM, Spetzler HA, Getting IC (1984) Capacitance transducer with a point-like probe for receiving acoustic emissions. Rev Sci Instrum 55(8):1293–1297

Chen LH, Labuz JF (2006) Indentation of rock by wedge-shaped tools. Int J Rock Mech Min Sci 43:1022–1033

Davi R, Vavryčuk V, Charalampidou E, Kwiatek G (2013) Network sensor calibration for retrieving accurate moment tensors of acoustic emissions. Int J Rock Mech Min Sci 62:59–67

Fakhimi A, Carvalho F, Ishida T, Labuz JF (2002) Simulation of failure around a circular opening in rock. Int J Rock Mech Min Sci 39:507–515

Glaser SD, Weiss GG, Johnson LR (1998) Body waves recorded inside an elastic half-space by an embedded, wideband velocity sensor. J Acoust Soc Am 104:1404–1412

Goebel THW, Becker TR, Schorlemmer D, Stanchits S, Sammins C, Rybacki E, Dresen G (2012) Identifying fault heterogeneity through mapping spatial anomalies in acoustic emission statistics. J Geophys Res 117:B03310

Goodfellow S, Young R (2014) A laboratory acoustic emission experiment under in situ conditions. Geophys Res Lett 41:3422–3430

Graham CC, Stanchits S, Main IG, Dresen G (2010) Source analysis of acoustic emission data: a comparison of polarity and moment tensor inversion methods. Int J Rock Mech Min Sci 47:161–169

Grosse CU, Ohtsu M (eds) (2008) Acoustic emission testing. Springer, Berlin

Gutenberg B, Richter CF (1942) Earthquake magnitude, intensity, energy and acceleration. Bull Seismol Soc Am 32:163–191

Hardy HR Jr (1994) Geotechnical field applications of AE/MS techniques at the Pennsylvania State University: a historical review. NDT&E Int 27(4):191–200

Heap MJ, Baud P, Meredith PG, Bell AF, Main IG (2009) Time-dependent brittle creep in Darley Dale sandstone. J Geophys Res 114:B07203

Hardy HR Jr (2003) Acoustic emission/microseismic activity, vol 1. Principles, Techniques and Geotechnical Applications. Balkema/CRC Press, ISBN 9789058091932

Ishida T, Chen Q, Mizuta Y, Roegiers J-C (2004) Influence of fluid viscosity on the hydraulic fracturing mechanism. J Energy Resour Technol Trans ASME 126:190–200

Ishida T, Aoyagi K, Niwa T, Chen Y, Murata S, Chen Q, Nakayama Y (2012) Acoustic emission monitoring of hydraulic fracturing

laboratory experiment with supercritical and liquid CO_2. Geophys Res Lett 39:L16309
Kaiser J (1953) Erkenntnisse und Folgerungen aus der Messung von Geräuschen bei Zugbeanspruchung von metallischen Werkstoffen. Arch Eisenhüttenwes 24:43–45
Kanagawa T, Nakasa H (1978) Method of estimating ground pressure. US Patent No. 4107981
Kanagawa T, Hayashi M, Nakasa H (1976) Estimation of spatial components in rock samples using the Kaiser effect of acoustic emission. CRIEPI (Central Research Institute of Electric Power Industry) Report, E375004
Kao C-S, Carvalho FCS, Labuz JF (2011) Micromechanisms of fracture from acoustic emission. Int J Rock Mech Min Sci 48:666–673
Kasahara K (1981) Earthquake mechanics. Cambridge University Press, Cambridge, p 248
Kusunose K, Nishizawa O (1986) AE gap prior to local fracture of rock under uniaxial compression. J Phys Earth 34(Supplement):S45–S56
Kwiatek G, Plenkers K, Dresen G, JAGUARS Research Group (2011) Source parameters of picoseismicity recorded at Mponeng deep gold mine, South Africa: implications for scaling relations. Bull Seismol Soc Am 101:2592–2608
Kwiatek G, Charalampidou E, Dresen G, Stanchits S (2014) An improved method for seismic moment tensor inversion of acoustic emissions through assessment of sensor coupling and sensitivity to incidence angle. Int J Rock Mech Min Sci 65:153–161
Lavrov A (2003) The Kaiser effect in rocks: principles and stress estimation techniques. Int J Rock Mech Min Sci 40:151–171
Lei X, Nishizawa O, Kusunose K, Satoh T (1992) Fractal structure of the hypocenter distributions and focal mechanism solutions of acoustic emission in two granites of different grain sizes. J Phys Earth 40:617–634
Lei X, Kusunose K, Satoh T, Nishizawa O (2003) The hierarchical rupture process of a fault: an experimental study. Phys Earth Planet Inter 137:213–228
Lockner DA (1993) Role of acoustic emission in the study of rock fracture. Int J Rock Mech Min Soc Geomech Abstr 30:884–899
Lockner DA, Byerlee JD, Kuksenko V, Ponomarev A, Sidorin A (1991) Quasi-static fault growth and shear fracture energy in granite. Nature 350:39–42
Manthei G (2005) Characterization of acoustic emission sources in rock salt specimen under triaxial compression. Bull Seismol Soc Am 95(5):1674–1700
McLaskey G, Glaser S (2012) Acoustic emission sensor calibration for absolute source measurements. J Nondestruct Eval 31:157–168
McLaskey G, Kilgore B, Lockner D, Beeler N (2014) Laboratory generated M-6 earthquakes. Pure Appl Geophys 171:2601–2615
Mogi K (1962a) Study of the elastic shocks caused by the fracture of heterogeneous materials and its relation to earthquake phenomena. Bull Earthq Res Inst Tokyo Univ 40:125–173
Mogi K (1962b) Magnitude-frequency relation for elastic shocks accompanying fracture of various materials and some related to problems in earthquakes. Bull Earthquake Res Inst Tokyo Univ 40:831–853
Mogi K (1968) Source locations of elastic shocks in the fracturing process in rocks (1). Bull Earthquake Res Inst Tokyo Univ 46:1103–1125
Mogi K (2006) Experimental rock mechanics. Taylor & Francis, London
Nakayama Y, Inoue A, Tanaka M, Ishida T, Kanagawa T (1993) A laboratory experiment for development of acoustic methods to investigate condition changes induced by excavation around a chamber. Proc Third Int Symp Rockburst Seism Mines, Kingston, pp 383–386
Nasseri MHB, Mohanty B, Young RP (2006) Fracture toughness measurements and acoustic emission activity in brittle rocks. Pure Appl Geophys 163:917–945
Nasseri MHB, Goodfellow SD, Lombos L, Young RP (2014) 3-D transport and acoustic properties of Fontainebleau sandstone during true-triaxial deformation experiments. Int J Rock Mech Min Sci 69:1–18
Nishizawa O, Onai K, Kusunose K (1984) Hypocenter distribution and focal mechanism of AE events during two stress stage creep in Yugawara andesite. Pure Appl Geophys 112:36–52
Obert L, Duvall WI (1945) Microseismic method of predicting rock failure in underground mining "Part II, Laboratory experiments", RI 3803, USBM
Ohtsu M, Ono K (1986) The generalized theory and source representations of acoustic emission. J Acoust Emiss 5(4):124–133
Proctor T (1982) An improved piezoelectric acoustic emission transducer. J Acoust Soc Am 71:1163–1168
Salamon MDG, Wiebols GA (1974) Digital location of seismic events by an underground network of seismometers using the arrival times of compressional waves. Rock Mech 6(2):141–166
Scholz CH (1968a) The frequency-magnitude relation of microfracturing in rock and its relation to earthquake. Bull Seismol Soc Am 58:399–415
Scholz CH (1968b) Microfracturing and the inelastic deformation of rock in compression. J Geophys Res 73(4):1417–1432
Scholz CH (1968c) Experimental study of the fracturing process in brittle rock. J Geophys Res 73(4):1447–1454
Scholz CH (2002) The mechanics of earthquakes and faulting, 2nd edn. Cambridge University Press, Cambridge
Sellers EJ, Kataka MO, Linzer LM (2003) Source parameters of acoustic emission events and scaling with mining. J Geophys Res 108(B9):2418–2433
Shah KR, Labuz JF (1995) Damage mechanisms in stressed rock from acoustic emission. J Geophys Res 100(B8):15527–15539
Shearer PM (2009) Introduction to seismology, 2nd edn. Cambridge University Press, Cambridge
Spetzler H, Sobolev G, Koltsov A, Zang A, Getting IC (1991) Some properties of unstable slip on rough surfaces. Pure Appl Geophys 137:95–112
Stanchits S, Mayr S, Shapiro S, Dresen G (2011) Fracturing of porous rock induced by fluid injection. Tectonophysics 503(1–2):129–145
Stanchits S, Surdi A, Gathogo P, Edelman E, Suarez-Rivera R (2014) Onset of hydraulic fracture initiation monitored by acoustic emission and volumetric deformation measurements. Rock Mech Rock Eng 47(5):1521–1532
Stein S, Wysession M (2003) An introduction to seismology, earthquakes, and earth structure. Blackwell, Malden
Stierle E, Vavryčuk V, Kwiatek G, Charalampidou E, Bohnhoff M (2016) Seismic moment tensors of acoustic emissions recorded during laboratory rock deformation experiments: sensitivity to attenuation and anisotropy. Geophys J Int 205:38–50
Terada M, Yanagidani T, Ehara S (1984) AE rate controlled compression test of rocks. In: Hardy HR Jr, Leighton FW (eds) Proceedings of third conference on acoustic emission/microseismic activity in geologic structure and materials. Trans Tech Publication, University Park, pp 159–171
Thompson BD, Young RP, Lockner DA (2005) Observations of premonitory acoustic emission on slip nucleation during a stick slip experiment in smooth faulted Westerly granite. Geophys Res Lett 32:L10304
Thompson BD, Young RP, Lockner DA (2006) Fracture in Westerly granite under AE feedback and constant strain rate loading:

nucleation, quasi-static propagation, and the transition to unstable fracture propagation. Pure Appl Geophys 163:995–1019

Xiao Y, Feng X, Hudson JA, Chen B, Feng G, Liu J (2016) ISRM suggested method for in situ microseismic monitoring of the fractured process in rock masses. Rock Mech Rock Eng 49:843–869

Yanagidani T, Ehara S, Nishizawa O, Kusunose K, Terada M (1985) Localization of dilatancy in Ohshima granite under constant uniaxial stress. J Geophys Res 90(B8):6840–6858

Yoshimitsu N, Kawakata H, Takahashi N (2014) Magnitude-7 level earthquakes: a new lower limit of self-similarity in seismic scaling relationship. Geophys Res Lett 41:4495–4502

Zang A, Wagner FC, Dresen G (1996) Acoustic emission, microstructure, and damage model of dry and wet sandstone stressed to failure. J Geophys Res 101(B8):17507–17521

Zang A, Wagner FC, Stanchits S, Dresen G, Andresen R, Haidekker MA (1998) Source analysis of acoustic emissions in Aue granite cores under symmetric and asymmetric compressive loads. Geophys J Int 135:1113–1130

Zang A, Wagner FC, Stanchits S, Janssen C, Dresen G (2000) Fracture process zone in granite. J Geophys Res 105(B10):23651–23661

Zietlow WK, Labuz JF (1998) Measurement of the intrinsic process zone in rock using acoustic emission. Int J Rock Mech Min Sci 35(3):291–299